Optics Letters

Synthetic aperture rainbow refractometry

Xinhao Wang,[1,2] Yingchun Wu,[1,2,*] Dongyan Xu,[1] Botong Wen,[1] Qimeng Lv,[1] and Xuecheng Wu[1]

[1] State Key Laboratory of Clean Energy Utilization, Zhejiang University, Hangzhou 310027, China
[2] Huzhou Institute of Zhejiang University, Huzhou 313000, China
*Corresponding author: wuyingchun@zju.edu.cn

Received 21 July 2022; revised 18 September 2022; accepted 20 September 2022; posted 20 September 2022; published 4 October 2022

This work proposed a synthetic aperture rainbow refractometry (SARR) by synthesizing rainbow signals of the same droplet with dual-wavelength laser beams, in order to increase the aperture of rainbow refractometry. In this way, the SARR can apply to long distance and small droplets measurement. An achromatic imaging system, which simultaneously records while separating the two rainbow signals in two channels of a color image, is elaborately designed. A data processing algorithm is developed to retrieve the optimal droplet refractive index and size. Numerical simulations of different droplet sizes from 10 μm to 200 μm certify the viability of the SARR. Proof-of-concept experiments of micron-sized ethanol droplets are performed with 1650 mm measurement distance. Results show that the SARR can accurately measure droplet refractive index and size with uncertainties of 2.3×10^{-4} and 2 μm, respectively. The feasibility and accuracy of the proposed SARR are successfully demonstrated, paving the way for rainbow refractometry applied to large-scale industrial applications.

https://doi.org/10.1364/OL.471103

Rainbow refractometry takes a unique and important role in droplet measurement due to the capability of simultaneously measuring droplet size [1,2], refractive index (RI) [3], temperature, constitution [4], surface tension [5], and so on, by analyzing the angular position and distribution of light scattering around the geometric rainbow angle. In the past three decades, rainbow refractometries have developed several variations. The initial form was standard rainbow refractometry for single droplet and monodispersed droplet stream measurement [1], and later evolved to global rainbow refractometry to measure average refractive index and size distribution of a cloud of multi-dispersed droplets [3]. Afterwards, rainbow refractometries were proposed to extend the measurement area from a single point to a line segment even to a plane, called one-dimensional rainbow refractometry [2,6] and planar rainbow refractometry [7]. Phase rainbow refractometry [8,9] was developed to measure the nanoscale size variation of evaporating droplets from the phase shift of the high frequency ripple structure of rainbow signals. In addition, rainbow refractometries have been extensively applied to a variety of laboratory and industrial conditions for some time [10–12], including sprays [13–15], evaporation, combustion [16,17], spray mixing of binary sprays [18], and even three sprays [4]. A dual-wavelength extinction rainbow refractometry [19] was used to investigate inclusion concentration in colloidal droplets. However, the above rainbow refractometries, typically used to measure droplets from 50 μm to 500 μm, are limited in applications due to their insufficient measuring distance and small range. Especially in some large-scale industrial scenarios such as icing wind tunnels, desulfurization towers in coal-fired power plants, the measurement distance should be larger than 1000 mm. As for high-pressure industrial environments such as combustion chambers in aircraft engines, droplets have size of tens of microns and large temperature variations. Considering that the applied industrial environments become increasingly complicated and hostile [20], rainbow refractometry needs development for the relatively large scale of industrial facilities and droplets with small size.

The backward scattering configuration of rainbow refractometry fits for the industrial cases described above, but the core difficulty is the limited optical aperture for both long distance and small droplets measurement. In general, the aperture of the recorded rainbow signal should cover the region from the Alexander dark band to the end of the main peak. The width of the main peak is approximately $\frac{4}{3}\left(\theta_f - \theta_{rb}\right)$. Here θ_{rb} is the geometric rainbow angle, and θ_f is a special angle where the light intensity is minimal in the range from the main peak to the first supernumerary bow. Now $\theta_f - \theta_{rb}$ can be expressed as

$$\theta_f - \theta_{rb} = \frac{816}{349} \frac{\left(4 - n^2\right)^{\frac{1}{6}}}{\left(n^2 - 1\right)^{\frac{1}{2}}} \left(\frac{3}{\lambda d}\right)^{\frac{2}{3}}, \tag{1}$$

where n and d represent RI and diameter of droplet, respectively, and λ is the laser wavelength. For instance, the aperture of rainbow refractometry should gather at least 4.5° for a droplet with diameter of 150 μm, implying that the measurement distance is at large 850 mm on the premise of common optical components of 4 in. This measurement distance satisfies most laboratory applications, while it fails in industrial scenarios. Especially the world-class large icing wind tunnels [21–23] have a test section up to 3 m × 2 m, so in order to measure cloud droplet at the center, a stand-off distance requires larger than 1500 mm. Non-intrusive techniques facilitate cloud droplet measurement located outside of the wind tunnels and are favorable, for interferometric particle imaging [24], where the diameter of a supercooled large droplet is larger than 100 μm. This Letter proposes a synthetic aperture rainbow refractometry, which

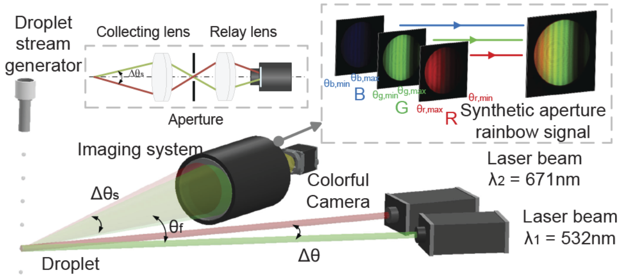

Fig. 1. Optical principles and light path of synthetic aperture rainbow refractometry, and the diagram of multi-channel image synthesis.

increases the aperture of the rainbow refractometry by collecting different rainbow signals with a color camera.

Synthetic aperture rainbow refractometry can use multiple laser beams, and the details with dual-wavelength laser beams are presented in this work. Figure 1 illustrates the optical principles and light path of the synthetic aperture rainbow refractometry with two lasers, and the diagram of multi-channel image synthesis. Two laser beams with different wavelengths of λ_1 and λ_2 are converged to the measurement point with different incident angles, with a crossing angle of $\Delta\theta$, and then scattered by droplets to form stable dual-wavelength rainbow signals. An achromatic imaging system collects the rainbow signals with aperture of $\Delta\theta_s = (\theta_{\max} - \theta_{\min})$, where $\theta_{\min}$ and $\theta_{\max}$ are the lower and upper bound of the recording scattering angle of rainbow light with wavelength λ_1. Two superimposed rainbow signals, $\mathbf{I}(\lambda_1, [\theta_{\min}, \theta_{\max}])$ and $\mathbf{I}(\lambda_2, [\theta_{\min} - \Delta\theta, \theta_{\max} - \Delta\theta])$, are recorded by two different channels of a color industrial camera, composing a synthetic aperture rainbow signal, noted as $\mathbf{I}_{SA}(\lambda, \theta)$, as follows:

$$\mathbf{I}_{SA}(\lambda, \theta) = \mathbf{I}(\lambda_1, [\theta_{\min}, \theta_{\max}]) + \mathbf{I}(\lambda_2, [\theta_{\min} - \Delta\theta, \theta_{\max} - \Delta\theta]) . \quad (2)$$

Equation (2) reveals that the light scattering around rainbow spanning $[\theta_{\min} - \Delta\theta, \theta_{\max}]$ is recorded, with an increase of $\Delta\theta$ in aperture. Thus, the proposed technique combines two rainbow refractometries of different wavelengths and scattering angles, and can be called a synthetic aperture rainbow refractometry (SARR) or synthetic aperture rainbow refraction spectroscopy (SARRS), and is hereinafter referred to as SARR. There are several merits in SARR in this configuration.

- The intersection of two laser beams coincides with the measurement point, facilitating its location and absolute scattering angle calibration.
- Two rainbow signals share a common recording imaging system, and this eliminates errors in optical imaging, e.g., scattering angle-image pixel calibration.
- Two rainbow signals are recorded by the same imaging system, and this ensures the sampled droplets are the same.

Yet it is worth mentioning the chromatic dispersion, which means the droplet RI changes with laser wavelength, and should be carefully tackled in SARR. An achromatic imaging system is necessary to eliminate dispersion and chromatic aberration, otherwise the sampling volume varies for two rainbow signals. Subsequently, the rainbow angle shifts with laser wavelength, and this should be considered in both rainbow signals recording and inversion. In addition, $\Delta\theta$ is usually smaller than the aperture $\Delta\theta_s$ for the overlapping of two rainbow signals.

In order to verify the feasibility of the SARR, synthetic aperture rainbow signals of different sizes are simulated using the Lorenz–Mie theory [25], and then analyzed for accuracy validation. The RI is 1.3637 corresponding to that of an ethanol droplet at a temperature of 20°C for the laser wavelength of 532 nm, and several sizes of ethanol droplets are set as d = 10 µm, 15 µm, 20 µm, 25 µm, 30 µm, 35 µm, 40 µm, 50 µm, 75 µm, 100 µm, 125 µm, 150 µm, 175 µm, and 200 µm. Samples from 10 µm to 50 µm are selected and simulated to validate small droplet measurement of the SARR. The solid lines in Fig. 2 illustrate a typical normalized synthetic aperture rainbow signal of an ethanol droplet with d = 100 µm. The scattering light intensity near the geometric rainbow angle is intercepted from the curve of wavelength λ_2 = 671 nm, covering the scattering angle (138.7° to 142.9°) for d = 100 µm. Next the wavelength λ_1 = 532 nm curve is chosen to describe the main peak to the first supernumerary, where the scattering angle is from 141.4° to 145.7°. Both parts form a synthetic aperture rainbow signal with the aperture of 4.2° for an individual laser beam, and each covers half of the complete rainbow pattern at least. The solid lines in Fig. 2 show the positions of two rainbow signals are slightly shifted, angles of main peaks are less than 1°, and the normalization light intensity is basically identical.

Assuming droplets are homogeneous and spherical and ignoring the interference of light scattering among droplets, the droplet RI and diameter can be simultaneously inversed from a SARR signal, by finding the optimal fitting of the recorded SARR signal as follows:

$$\arg\min_{n,d} \left\{ \left\| \begin{array}{l} \mathbf{I}_{SA}(\lambda, \theta) - c_1 \mathbf{I}_{fit}\left(n_{\lambda_1}, [\theta_{\min}, \theta_{\max}], d\right) \\ -c_2 \mathbf{I}_{fit}\left(n_{\lambda_1} - \Delta n, [\theta_{\min} - \Delta\theta, \theta_{\max} - \Delta\theta], d\right) \end{array} \right\| \right\}, \quad (3)$$

where the coefficients $c_{1,2}$ are presented to reduce the effects of different light intensities from two laser beams. Two candidate rainbow signals $\mathrm{I}_{fit}\left(n_{\lambda_1}, [\theta_{\min}, \theta_{\max}], d\right)$ and $\mathrm{I}_{fit}\left(n_{\lambda_2}, [\theta_{\min} - \Delta\theta, \theta_{\max} - \Delta\theta], d\right)$ are computed according to the complex angular momentum (CAM) theory [26,27]. The refractive index difference for two laser beams is computed with the dispersion relationship

$$\Delta n = n_{\lambda_1} - n_{\lambda_2} = A \cdot \left(\lambda_1^{-2} - \lambda_2^{-2}\right) + B \cdot \left(\lambda_1^{-4} - \lambda_2^{-4}\right), \quad (4)$$

where the coefficients A and B change with droplet composition, and specific assignments are stated in Ref. [28]. For ethanol droplets at a temperature of 20°C, the coefficients of n_{λ_1} versus

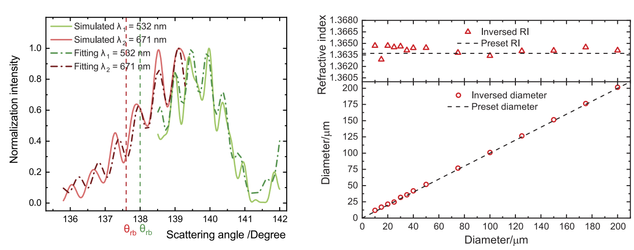

Fig. 2. (a) Normalized synthetic aperture rainbow intensity and its fitting with wavelength of λ_1 = 532 nm and λ_2 = 671 nm, and d = 100 µm and n = 1.3637 for the laser λ_1. (b) Comparison of refractive index and diameter values for the laser λ_1 from preset and inversion.

n_{λ_2} are $A = 3.06 \times 10^{-3}$, $B = 2.00 \times 10^{-5}$. The minimization of Eq. (3) is achieved by a constrained multi-objective optimization algorithm with RI and diameter of physical meaning.

Droplet RI and diameter are deduced from the simulated synthetic aperture rainbow signals with the developed algorithm, as displayed in Fig. 2. The fitting of simulated rainbow signals of the laser $\lambda_1 = 532$ nm and $\lambda_2 = 671$ nm is plotted by the dotted lines of Fig. 2, which matches well at both the rainbow geometric angle and the main peak. Then the average value of refractive index is 1.3642 for laser $\lambda_1 = 532$ nm with a deviation of 5×10^{-4}. As for droplet size, the average error of these tests is less than 2 μm. The differences between the inversed values from the SARR and the theoretical values [28,29] of RI and size were calculated and averaged to obtain the uncertainty of corresponding parameters. A comparison of the inversed and preset values of RI and diameter are demonstrated in Fig. 2, respectively. Apparently, the calculated values are quite close to the explicit values imported during simulation, and root mean square (RMS) errors between both access are within the allowable range of engineering error, which is 8.33×10^{-4} and 2 μm for RI and diameter, respectively. As for small droplets, the simulated signals with diameter from 20 μm to 50 μm are handled excellently in Fig. 2 and the deviations between the preset and inversed values of size are less than that from 10 μm to 20 μm. Therefore, it is possible for SARR to measure small droplet with high accuracy.

The experimental setup of synthetic aperture rainbow refractometry consisted of two lasers with wavelengths of 532 nm and 671 nm, and an achromatic Fourier imaging system for rainbow signal recording. Both lasers were vertically polarized and the imaging system captured the perpendicular polarization of rainbow light intensity for high precision. The measurement point was the intersection of two laser beams, and it was convenient to mark a measurement point while using a mirror to calibrate the scattering angle so that the step of setting up an additional laser could be skipped. The achromatic Fourier imaging system mainly involved a collecting lens, an aperture, an relay lens, and a color camera. The collecting lens and relay lens constituted a Fourier imaging system, ensuring that the light incident position recorded by the camera is only sensitive to the scattering angle. The collecting lens and the pinhole aperture with diameter of 2 mm formed a spatial filtering system removing background noise and interference and improving rainbow image quality. Both the collecting lens and the relay lens were achromatic. The color camera had a sensor size of 11.3 *mm* × 11.3 *mm* with resolution of 2040 pixels × 2046 pixels. There was a clear distinction between the spectral response lied on $\lambda_1 = 532$ nm and $\lambda_2 = 671$ nm of this color camera [30], and the interaction of two laser beams can be ignored. So two rainbow signals were separated just by extracting light distribution from different channels for inversion. The measurement distance was 1650 mm and the collecting angle was 2.5° calculated by the relationship of lens size and measurement distance.

A homogeneous monodispersed ethanol droplet stream was generated through a self-developed monodispersed droplet stream generator (MDSG), and the variation of droplet size was achieved by adjusting the generator. The distance from the measurement point to the outlet of the MDSG was 20 mm to avoid the influence of droplet oscillation and evaporation. The droplet size from MDSG of five test cases is 124 μm, 134 μm, 152 μm, 162 μm, and 185 μm. The ethanol droplets of different diameters are measured with the synthetic aperture

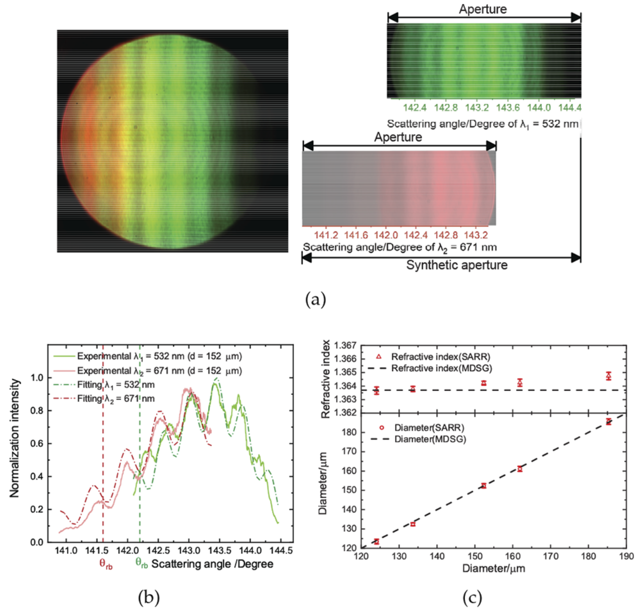

Fig. 3. (a) Synthetic aperture rainbow image of monodispersed ethanol droplet with a diameter of 152 μm. (b) Normalized light intensity distribution of the synthetic aperture rainbow signal and its fitting from panel (a). (c) Comparison of refractive index and diameter values from the experiment.

rainbow refractometry. Figure 3 displays an experimental synthetic aperture rainbow image and two monochrome rainbow signals. It is clear that two main peaks of rainbow signals are distributed on different positions, attributing to the two laser wavelengths and different incident angles. The scattering angle of the green rainbow signal is from 142° to 144.5° and that of red is from 141° to 143.5°. It is obvious to distinguish the locations of the main peak, the Alexander band and the ripple structure. The solid lines in Fig. 3 are the normalized intensity distribution of laser wavelength $\lambda_1 = 532$ nm and $\lambda_2 = 671$ nm corresponding to the upper and lower abscissas. It is intuitive the imaging angle range of the device is 2.5° for an individual laser beam. The equivalent aperture is more than twice the original size. It is obvious that a 2.5° collection scope is impossible to carry refractive index and diameter information but the synthetic aperture rainbow breaks this limit. In this apparatus layout, the rainbow signal of green laser displays details from the main peak to the first supernumerary, while the curve of red one covers the transition area from the Alexander dark band to the main peak, in which way two broken rainbow patterns compose a complete rainbow signal.

The dotted lines in Fig. 3 represent the comparison of normalization intensity from the inversed synthetic aperture rainbow signal, and such fitted circumstances in the figure would pledge the dependability and precision of the inversion algorithm and synthetic aperture rainbow refractometry at the same time. With these premises in mind, the course of processing two fractional rainbow signals is processed and aimed to handle a great amount test data in bulk. For the purpose of making the most of rainbow signals captured as much as possible, the 200 rows of pixels in the middle of rainbow pattern was normalized and calculated to provide droplet refractive index and diameter in each image. Not only distraction caused by spherical aberration and platform instability is reduced, but the sampling volume is sufficient to avoid randomness.

While the temperature of ethanol droplets is 20°C, the refractive index corresponding to the wavelength of 532 nm is 1.3637 [28]. Meanwhile, the refractive index value measured by synthetic aperture rainbow refractometry is 1.3641 for $\lambda_1 = 532$ nm, where the difference appears in the fifth decimal place, especially the RI from $d = 124$ µm is 1.3637. The RMS error is 2.3×10^{-4}, which matches the measurement accuracy in the laser polarization verification test. All of these can be intuitively understood in Fig. 3, and the similar information for size measurement is also aggregated. The maximum deviation of diameter is 2 µm from $d = 134$ µm, and the errors of left tests are basically within 2 µm. The average RMS error is 1 µm, which means inversed values are approximate to the parameters obtained from the MDSG. The reliability of the calculated diameter value from the MDSG has been verified [29]. Furthermore, the monochromatic signals separated from test images are processed to obtain droplet refractive index and diameter with more errors than the SARR. Both the numerical and experimental results demonstrate the feasibility of measuring droplets refractive index and diameter through the synthetic aperture rainbow refractometry, still maintaining high precision.

In order to conquer the incapability of rainbow refractometries in measuring a large range of droplet parameters at long distance resulting from the limited aperture of the achromatic imaging system, this work proposes a variation of rainbow refractometry, the synthetic aperture rainbow refractometry. SARR enlarges the aperture using the spectroscopic imaging of two rainbow signals from the same droplet illuminated by two laser beams of different wavelengths, and the proposed concept can be extended to three and more wavelengths for a further increase of aperture.

- The inversion algorithm is presented to process two incomplete rainbow patterns and the reliability and precision were proved through handling simulated signals.
- SARR is certified to measure droplets with different sizes from simulation especially sizes down to 10 µm.
- The monodispersed spherical ethanol droplet stream with different diameters are successfully measured at the 1650 mm distance.

In the experimental validation, the inversed values of RI and diameter are passable with uncertainty of 2.3×10^{-4} and 2 µm, respectively. The SARR takes advantages in many industrial applications, because of the measurement capabilities highlighted in this work. The non-sphericity of droplet significantly influences the measurement precision. SARR can satisfy internal measurement of large industrial equipment with a width of approximately 3000 mm, measure small droplets, and detect great temperature variations. As for sprays, the synthetic aperture rainbow refractometry will also work well as a global synthetic aperture rainbow refractometry. While it is used in combination with one-dimensional rainbow refractometry, planar rainbow refractometry, phase rainbow refractometry, consequential function, and applications must be satisfactory and suitable for more diverse measurement conditions.

Funding. National Science and Technology Major Project (J2019-III-0006-0049).

Disclosures. The authors declare no conflicts of interest.

Data availability. Data underlying the results presented in this paper are not publicly available at this time but may be obtained from the authors upon reasonable request.

REFERENCES

1. N. Roth, K. Anders, and A. Frohn, J. Laser Appl. **2**, 37 (1990).
2. X. Wu, H. Jiang, Y. Wu, J. Song, G. Gréhan, S. Saengkaew, L. Chen, X. Gao, and K. Cen, Opt. Lett. **39**, 638 (2014).
3. J. van Beeck, D. Giannoulis, L. Zimmer, and M. Riethmuller, Opt. Lett. **24**, 1696 (1999).
4. Y. Wu, C. Li, J. Cao, X. Wu, S. Saengkaew, L. Chen, G. Gréhan, and K. Cen, Exp. Therm. Fluid Sci. **98**, 309 (2018).
5. Q. Lv, Y. Wu, C. Li, X. Wu, L. Chen, and K. Cen, Opt. Lett. **45**, 6687 (2020).
6. J. Promvongsa, P. Vallikul, B. Fungtammasan, A. Garo, G. Grehan, and S. Saengkaew, Proc. Combust. Inst. **36**, 2401 (2017).
7. C. Li, Q. Lv, N. Li, Y. Wu, X. Wu, C. Weng, and C. Tropea, Opt. Lett. **46**, 5898 (2021).
8. Y. Wu, J. Promvongsa, S. Saengkaew, X. Wu, J. Chen, and G. Gréhan, Opt. Lett. **41**, 4672 (2016).
9. Y. Wu, H. Li, M. Brunel, J. Chen, G. Gréhan, and L. Mädler, Appl. Phys. Lett. **111**, 041905 (2017).
10. K. F. Ren, F. Onofri, C. Rozé, and T. Girasole, Opt. Lett. **36**, 370 (2011).
11. H. Yu, F. Xu, and C. Tropea, Opt. Express **21**, 25761 (2013).
12. F. R. Onofri, K. F. Ren, M. Sentis, Q. Gaubert, and C. Pelcé, Opt. Express **23**, 15768 (2015).
13. M. R. Vetrano, J. P. A. van Beeck, and M. L. Riethmuller, Appl. Opt. **43**, 3600 (2004).
14. M. R. Vetrano, S. Gauthier, J. van Beeck, P. Boulet, and J.-M. Buchlin, Exp. Fluids **40**, 15 (2006).
15. V. Bodoc, C. Laurent, Y. Biscos, and G. Lavergne, *Aerospace Lab* 1 (2009).
16. J. Wilms, G. Gréhan, and G. Lavergne, Part. Part. Syst. Charact. **25**, 39 (2008).
17. C. T. Wanstall, A. K. Agrawal, and J. A. Bittle, Appl. Opt. **58**, 6791 (2019).
18. J. Wilms and B. Weigand, Appl. Opt. **46**, 2109 (2007).
19. C. Li, Q. Lv, N. Li, Y. Wu, X. Wu, C. Weng, and C. Tropea, Powder Technol. **399**, 117098 (2022).
20. P. Lemaitre, G. Grehan, E. Porcheron, J. Malet, P. Cornet, P. Brun, and J. Vendel, in *9th International Conference on Liquid Atomization and Spray Systems*, Sorrento, Italy, July 13–17, 2003.
21. T. Irvine, S. Kevdzija, D. Sheldon, and D. Spera, in *39th Aerospace Sciences Meeting and Exhibit* (American Institute of Aeronautics and Astronautics, 2001), 229.
22. L. Vecchione and P. De Matteis, in *41st Aerospace Sciences Meeting and Exhibit* (American Institute of Aeronautics and Astronautics, 2003), 900.
23. G. Xiangdong, L. Qinglin, L. Qingren, Y. Shengke, and Z. Zhao, Acta Aerodynamica Sinica **39**, 184 (2021).
24. A. Garcia-Magarino, S. Sor, R. Bardera, and J. Munoz-Campillejo, Measurement **168**, 108418 (2021).
25. P. Laven, J. Quant. Spectrosc. Radiat. Transfer **89**, 257 (2004).
26. H. Nussenzveig, J. Math. Phys. **10**, 125 (1969).
27. S. Saengkaew, T. Charinpanitkul, H. Vanisri, W. Tanthapanichakoon, L. Mees, G. Gouesbet, and G. Grehan, Opt. Commun. **259**, 7 (2006).
28. J. Rheims, J. Köser, and T. Wriedt, Meas. Sci. Technol. **8**, 601 (1997).
29. X. Wu, Q. Lv, Y. Wu, C. Li, and K. Cen, Chem. Eng. Sci. **223**, 115645 (2020).
30. "The spectral response of camera," https://docs.baslerweb.com/aca2040-90uc.